Sharif University of Technology

Scientia Iranica

Transactions on Nanotechnology

https://scientiairanica.sharif.edu

Entropy optimization of non-Newtonian hybrid nanofluid flow with non-linear radiation, exponential and thermal-dependent heat source: Neuro-intelligent design

Abbai Reddy Divya, Polu Bala Anki Reddy *

Department of Mathematics, School of Advanced Sciences, Vellore Institute of Technology (VIT), Vellore, Tamil Nadu-632014, India.

* Corresponding author: pbarmaths@gmail.com (P. Bala Anki Reddy)

Received 07 November 2022; received in revised form 17 February 2023; accepted 18 June 2023

Keywords

Electromagnetohydrodynamic flow;

Thermal and exponential space dependent heat source;

Artificial neural network model;

Oldroyd-B fluid;

Entropy generation.

Abstract

The prediction of entropy generation with a thermal and exponential space dependent heat source of unsteady flow over a rotating disk is the artifact of the paper. For the specific physical model, Oldroyd-B within fluid flow is encrypted. Also, mechanism of cobalt and tantalum nanoparticles with in the blood is employed. The proper self-similarity variables are used to convert the non-linear PDE system of equations into an ODE form, which is then calculated using the Runge–Kutta 4th with shooting technique and artificial neural network. Visual representations are used to show how different skewing interact with each other. With a few exceptions, the research findings of the model are quite consistent with those reported in the literature. Skin frictions decrease for the parameters like radiation, Eckert number, Brinkman number and exponential based heat source. Nusselt number rises for electric and unsteady parameters. Also, entropy generation rises for magnetic field and Brinkman number whereas opposite tendency is observed for the electric field. Since cobalt stimulates red blood cell production, while tantalum is employed in bone implants and iodinated agents for blood imaging due to its long circulation time. Thus, this research may be used to treat anemia.

1. Introduction

In comparison to Newtonian materials, non-Newtonian materials have become more prevalent in the mechanical, commercial and industrial areas in recent decades. This is due to the fact that Newtonian fluids cannot predict elastic characteristics, but non-Newtonian fluids can possesses the highest viscoelastic property [1]. Mud, ketchup, glues, blood, fiber, mineral oils, ink, shampoos, chemical solutions, paints, exotic lubricants, cosmetics, annealing of copper wire, colloids and suspensions, clay coatings, coal water and a range of other thin and thick substances behave like non-Newtonian fluids and are treated as such kind [2,3]. Furthermore, such fluids are employed in synthetic processes, oil store construction, culinary products, material handling and in the multitude of different applications [4]. For the most part of non-Newtonian fluids, they are divided into three categories: differential, rate, and integral. The stress relaxation and creep processes are demonstrated by the fluids in rate type. One of that rate-type fluids is represented by the Oldroyd-B model, which is an extension of the upper convicted viscoelastic Maxwell fluid model with retardation time. Oldroyd-B [5] investigated this model of fluid. Actually, the progression of Oldroyd-B fluid is more suited to fit the rheological data rather than other non-Newtonian models, according to a literature review [6]. Khan et al. [7] investigated the Oldroyd-B fluid flow using Karman transformations to formulate the problem over a rotating disk. The investigation of Oldroyd-B nanofluid with cross diffusion effects was did by Khan et al. [7] and he discovered that the dufour effect enhances the thermal profile. Hafeez et al. [4] recently investigated Oldroyd-B fluid flow which is chemically reactive with Cattaneo–Christov heat flux theory over a rotating disk. Shivakumara and SureshKumar [8] investigated Oldroyd-B fluid with the effects of flow and quadratic drag on the stability in a region of porous.

Chemical or nuclear processes generate heat energy within a body as an interior energy source/sink. Its significance may be observed in combustion research, heat exchangers, production of plastic, thermal insulation, fusion reactors, paper and steel manufacturing, nuclear reactors, among other things. The effects of an internal heat source/sink may be studied using two models. The first is a uniform temperature dependent internal

To cite this article:

A. Reddy Divya, and P. Bala Anki Reddy "Entropy optimization of non-Newtonian hybrid nanofluid flow with non-linear radiation, exponential and thermal-dependent heat source: Neuro-intelligent design", *Scientia Iranica* (2025), **32**(3):7291. https://doi.org/10.24200/sci.2023.61412.7291

heat source/sink process, while the second is a non-uniform space. In general, Thermal based Heat Source (THS) has two dimensionless components which is encrypted in the energy equation, one for analyzing THS and the other for analyzing space based heat sources [9]. But these two models may not be able to accomplish more heat transmission in the fluid boundary layer, according to science. So, an Exponential Space-based Heat Source (ESHS) effect has been developed as a novel model for intensive heating processes in light of these findings. Khan et al. [10] studied irregular heat source with Marangoni convective flow over a disk which is rotating. Mahanthesh et al. [11] performed MHD flow with thermal and exponential space dependent heat source of SWCNT and MWCNT nanofluid over a rotating stretchable disk. Radiation on Maxwell fluid with in MWCNT nanotube was investigated by Fatehinasab et al. [12] and Ferdosi et al.[13].

Entropy generation or production is the rate of heat transfer in any irreversible process. Usually, diffusion, Joule heating, chemical reactions, flow of heat through thermal resistance, fluid's viscosity, friction of solid surfaces are some of the irreversible processes that produce entropy. Although there are numerous reasons for entropy generation in this process, some of those can be named as heat exchange, fluid movement, mixing and expansion of substances, solid deformation, motion of bodies or any irreversible thermodynamic cycle. For example, heat pumps, air conditioners, heat engines, power plants and so on [10]. Jakeer and Reddy [14] investigated entropy generation of a hybrid nanofluid with electromagnetohydrodynamic (EMHD) stagnation point. Khan et al. [15] investigated the dynamics of MHD nanomaterial in three dimensional flow with entropy generation between two rotating disks. Rashidi et al. [16] explored the entropy generation of MHD steady flow owing to a spinning porous disk.

Several research on the uses of Artificial Neural Network (ANN) in thermodynamics have been conducted in recent years. Reddy and Das [17] analyzed MHD boundary layer flow with chemical reaction employing a mix of ANN modelling and numerical over a stretched cylinder. Raghu and Sriraam [18] explored the best configuration of a multilayer perceptron neural network classifier for detecting intracranial epileptic episodes. Hasan et al. [19] studied a heart disease related detection system through which Multi-Layer Perceptron neural network is used. Heidari et al. [20] developed a grasshopper optimization in the multilayer perceptron neural network for the hybrid.

To the best of the authors' knowledge, no research has been done on entropy generation in EMHD with a thermal and exponential space dependent heat source of unsteady flow over a rotating disk. The governing flow of non-linear partial differential equations are converted into a system of highly non-linear ordinary differential equations using appropriate similarity transformations, which are then numerically solved using a Runge–Kutta fourth order with shooting technique and then ANN is applied. To satisfy our criteria, we constructed the necessary graphs and tables for the established parameters. For this work, we used blood as

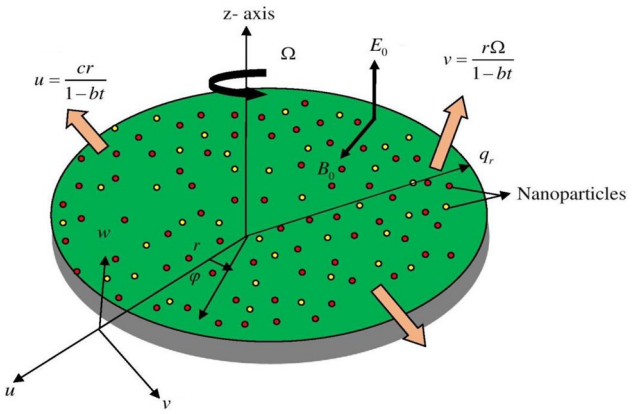

Figure 1. Geometry of the problem.

the base fluid and nano particles like tantalum and cobalt to enhance Oldroyd-B fluid. The current study aims to be useful in clinical applications where tantalum is used as a nanoparticle that is easily oxidized in the air due to its high reactivity, as well as in the treatment of microbial infections and since cobalt nanoparticles are nontoxic at low concentrations [21] and have minimal side effects than antibiotics.

2. Formulation of the problem

Consider a non-Newtonian Oldroyd-B fluid over a rotating disk with an unsteady EMHD conducting flow of hybrid nanofluid where the disk is stretchable. Also, non-linear thermal radiation and ESHS (irregular heat source/sink) is taken into an account. Here, disk rotates with an uniform magnetic field B_0 and has the angular velocity Ω which is placed at $z = 0$ as shown in Figure 1. The disk has a surface temperature termed as T_s and the temperature away from the disk as T_∞. For the solvation of this problem, the following presumptions are used:

$$u = \frac{cr}{(1-bt)}\,,\quad v = \frac{r\Omega}{(1-bt)}\,,\quad B(t) = \frac{B_0}{(1-bt)^{\frac{1}{2}}},$$

$$T_s = T_0 - T_{ref}\left(\frac{r^2\Omega}{\upsilon(1-bt)^{\frac{3}{2}}}\right). \tag{1}$$

The equations for continuity, momentum and energy that govern this form of flow are as follows [22-25]:

$$\frac{\partial w}{\partial z} + \frac{1}{r}\frac{\partial}{\partial r}(ur) = 0, \tag{2}$$

$$\left(\frac{\partial u}{\partial t} - \frac{v^2}{r} + w\frac{\partial u}{\partial z} + u\frac{\partial u}{\partial r}\right) = \upsilon_{hnf}\left(\frac{\partial^2 u}{\partial z^2}\right)$$

$$-\lambda_1\left[\begin{array}{l} u^2\left(\frac{\partial^2 u}{\partial r^2}\right) + w^2\frac{\partial^2 u}{\partial z^2} + 2uw\left(\frac{\partial^2 u}{\partial r \partial z}\right) - \\ \frac{2uv}{r}\left(\frac{\partial v}{\partial r}\right) - \frac{2vw}{r}\left(\frac{\partial v}{\partial z}\right) + \frac{uv^2}{r^2} + \frac{v^2}{r}\left(\frac{\partial u}{\partial r}\right) \end{array}\right]$$

$$+\upsilon_{hnf}\lambda_2\left[\begin{array}{l} \frac{-1}{r}\left(\frac{\partial u}{\partial z}\right)^2 - 2\left(\frac{\partial u}{\partial z}\right)\left(\frac{\partial^2 w}{\partial z^2}\right) + w\left(\frac{\partial^3 u}{\partial z^3}\right) - \left(\frac{\partial u}{\partial r}\right)\left(\frac{\partial^2 u}{\partial z^2}\right) - \\ \left(\frac{\partial u}{\partial z}\right)\left(\frac{\partial^2 u}{\partial r \partial z}\right) + u\left(\frac{\partial^3 u}{\partial r \partial z^2}\right) \end{array}\right]$$

$$+\frac{\sigma_{hnf}B_0}{\rho_{hnf}(1-bt)}(E_0 - B_0 u) - \frac{\upsilon_{hnf}}{k^*}u, \tag{3}$$

$$\left(\frac{\partial v}{\partial t}+\frac{uv}{r}+w\frac{\partial v}{\partial z}+u\frac{\partial v}{\partial r}\right)=\upsilon_{hnf}\left(\frac{\partial^2 v}{\partial z^2}\right)$$
$$-\lambda_1\begin{bmatrix}u^2\left(\frac{\partial^2 v}{\partial r^2}\right)+w^2\left(\frac{\partial^2 v}{\partial z^2}\right)+2uw\left(\frac{\partial^2 v}{\partial r\partial z}\right)+\\ \frac{2uv}{r}\left(\frac{\partial u}{\partial r}\right)+\frac{2vw}{r}\left(\frac{\partial u}{\partial z}\right)-2\frac{u^2 v}{r^2}-\frac{v^3}{r^2}\\ +\frac{v^2}{r}\left(\frac{\partial v}{\partial r}\right)\end{bmatrix}$$
$$+\upsilon_{hnf}\lambda_2\begin{bmatrix}u\left(\frac{\partial^3 v}{\partial r\partial z^2}\right)-2\left(\frac{\partial v}{\partial z}\right)\left(\frac{\partial^2 w}{\partial z^2}\right)+w\left(\frac{\partial^3 v}{\partial z^3}\right)\\ -\frac{1}{r}\left(\frac{\partial u}{\partial z}\right)\left(\frac{\partial v}{\partial z}\right)-\left(\frac{\partial v}{\partial r}\right)\left(\frac{\partial^2 u}{\partial z^2}\right)+\\ \frac{v}{r}\left(\frac{\partial^2 u}{\partial z^2}\right)-\left(\frac{\partial v}{\partial z}\right)\left(\frac{\partial^2 u}{\partial r\partial z}\right)-\frac{u}{r}\left(\frac{\partial^2 v}{\partial z^2}\right)\end{bmatrix}$$
$$+\frac{\sigma_{hnf}B_0}{\rho_{hnf}(1-bt)}(E_0-B_0 v)-\frac{\upsilon_{hnf}}{k^*}v, \quad (4)$$

$$\frac{\partial T}{\partial t}+u\frac{\partial T}{\partial r}+w\frac{\partial T}{\partial z}=\frac{k_{hnf}}{(\rho c_p)_{hnf}}\left(\frac{\partial^2 T}{\partial z^2}\right)$$
$$+\frac{\mu_{hnf}}{(\rho c_p)_{hnf}}\left[\left(\frac{\partial u}{\partial z}\right)^2+\left(\frac{\partial v}{\partial z}\right)^2\right]-\frac{16}{3}\frac{\sigma^*}{k^*(\rho c_p)_{hnf}}\frac{\partial}{\partial z}\left(T^3\frac{\partial T}{\partial z}\right)$$
$$+\frac{Q_T^*}{(\rho c_p)_{hnf}}(T-T_0)+\frac{Q_E^*(T_s-T_0)}{(\rho c_p)_{hnf}}exp(-n\sqrt{\frac{\Omega}{\upsilon}}z)$$
$$+\frac{\sigma_{hnf}}{(\rho c_p)_{hnf}(1-bt)}[E_0^2+B_0^2(u^2+v^2)]. \quad (5)$$

The Rosseland approximation may be used to represent the radiative heat flux, where σ^* and k^* are the Stefan Boltzmann and mean absorption coefficients, respectively.

$$q_r=-\frac{4\sigma^*}{3k^*}\frac{\partial T^4}{\partial z}=-\frac{16\sigma^* T^3}{3k^*}\frac{\partial T}{\partial z}\ . \quad (6)$$

The following are the similarity transformations:

$$u=\frac{r\Omega}{(1-bt)}f'(\eta),\ \ v=\frac{r\Omega}{(1-bt)}g(\eta),\ \ w=-2\left(\frac{\upsilon\Omega}{(1-bt)}\right)^{\frac{1}{2}}f(\eta),$$
$$\eta=\sqrt{\frac{\Omega}{\upsilon(1-bt)}}z,\ \ T=T_0-T_{ref}\frac{r^2\Omega}{\upsilon(1-bt)^{\frac{3}{2}}}\theta(\eta). \quad (7)$$

The boundary conditions are as follows:

$$u=\frac{cr}{1-bt},\ v=\frac{r\Omega}{1-bt},\ w=0,\ T=T_s \qquad \text{at}\ \ z=0$$
$$\frac{\partial u}{\partial z}=0,\ u\to 0\ ,\ \ \frac{\partial v}{\partial z}=0,\ v\to 0,\ T\to T_0\ \text{ as }\ z\to\infty. \quad (8)$$

The non-linear dimensionless equations are as follows:

$$\left(\frac{N_1}{N_3}\right)\beta_2(2f'^2-2ff'^v)+\left(\frac{N_1}{N_3}\right)f'''$$
$$-\beta_1(4fgg'+4f^2f'''-4ff'f'')-S(\frac{\eta}{2}f''+f')$$
$$+(g^2+2ff''-f'^2)-\left(\frac{N_1}{N_3}\right)\beta f'+\left(\frac{N_2}{N_3}\right)M(E_1-f')=0, \quad (9)$$
$$\left(\frac{N_1}{N_3}\right)\beta_2(2g'f''-2fg''')-\beta_1(4f'^2g+4f^2g''-4ff'g'$$
$$-4ff''g)-S(\frac{\eta}{2}g'+g)-2(g'f-f'g)+\left(\frac{N_1}{N_3}\right)g''$$
$$-\left(\frac{N_1}{N_3}\right)\beta g+\left(\frac{N_2}{N_3}\right)M[E_1-g]=0, \quad (10)$$

$$\left(\frac{N_4}{N_5}\right)\theta''+Rd\left(\frac{1}{N_5}\right)\left(\frac{4}{3}\right)\begin{Bmatrix}\theta''+(\theta_w-1)^3(3\theta^2\theta'^2+\theta^3\theta'')\\ +3(\theta_w-1)^2(2\theta\theta'^2+\theta^2\theta'')\\ +3(\theta_w-1)(\theta'^2+\theta\theta'')\end{Bmatrix}$$
$$+\left(\frac{N_1}{N_5}\right)Pr\,E\,c(f''^2+g'^2)+2\,Pr(f\theta'-\theta f')$$
$$-S\,Pr\left(\frac{3}{2}\theta+\frac{\eta}{2}\theta'\right)+\left(\frac{N_2}{N_5}\right)MEc\,Pr(f'^2+g^2+E_1^2)$$
$$+\left(\frac{1}{N_5}\right)Pr\,Q_t\,\theta+\left(\frac{1}{N_5}\right)Pr\,Q\,Exp(-n\xi)=0. \quad (11)$$

With the boundary conditions as:

$$f'=\omega,\ g=1,\ f=0,\ \theta=1, \qquad \text{at}\ \ \eta=0$$
$$f''\to 0,\ f'\to 0,\ g\to 0,\ g'\to 0,\ \theta\to 0\ \ \text{as}\ \ \eta\to\infty \quad (12)$$

The dimensionless parameters are as:

$$S=\frac{b}{\Omega}\,,\ \omega=\frac{c}{\Omega},\ \beta=\frac{\upsilon(1-bt)}{k^*\Omega},\ Pr=\frac{\mu_f(C_p)_f}{k_f},\ \beta_1=\frac{\lambda_1\Omega}{1-bt},$$
$$\beta_2=\frac{\lambda_2\Omega}{1-bt},\ Rd=\frac{4\sigma^*T_0^3}{k^*k_f},\ \theta_w=\frac{T_s}{T_0},\ Ec=\frac{r^2\Omega^2}{(1-bt)^2(\Delta T)(C_p)_f},$$
$$Q=\frac{Q_E^*(1-bt)}{(\rho c_p)\Omega},\ \xi=z\sqrt{\frac{\Omega}{\upsilon}},\ \ M=\left(\frac{\sigma_f B_0^2}{\rho_f\Omega}\right),\ Q_t=\frac{Q_T^*(1-bt)}{(\rho c_p)\Omega},$$
$$N_1=\frac{\mu_{hnf}}{\mu_f},\ N_2=\frac{\sigma_{hnf}}{\sigma_f},N_3=\frac{\rho_{hnf}}{\rho_f},N_4=\frac{k_{hnf}}{k_f},$$
$$N_5=\frac{(\rho C_p)_{hnf}}{(\rho C_p)_f},\ E_1=\left(\frac{E_0(1-bt)}{r\Omega B_0}\right).$$

3. Engineering interest quantities

The skin friction of both the velocities are defined as follows:

$$C_f=\frac{\tau_{w1}(1-bt)^2}{\rho_f(r\Omega)^2}, \quad (13)$$

$$C_g=\frac{\tau_{w2}(1-bt)^2}{\rho_f(r\Omega)^2}, \quad (14)$$

Here, $\tau_{w1}=\mu_{hnf}\left(\frac{\partial u}{\partial z}\right)_{z=0}$, $\tau_{w1}=\mu_{hnf}\left(\frac{\partial v}{\partial z}\right)_{z=0}$,

$$Re_x^{\frac{1}{2}}C_f=N_1f''(0), \quad (15)$$

$$Re_x^{\frac{1}{2}}C_g=N_1g'(0). \quad (16)$$

The heat transfer rate, often known as the Nusselt number, is the physical quantity of concern in this subject.

$$Nu_r=\frac{rq_w}{k_f(T_s-T_0)}\,, \quad (17)$$

where $q_w=\left(-k_{hnf}\left(\frac{\partial T}{\partial z}\right)_{z=0}\right)+\left(\frac{16\sigma^*T_\infty^3}{3k^*k_f}\right)_{z=0}$,

$$Nu_x\,Re_x^{-\frac{1}{2}}=-\left\{N_4+\tfrac{4}{3}Rd[1+(\theta_w-1)\theta(0)]^3\right\}\theta'(0), \quad (18)$$

where Re_x is the local Reynolds number and it can be written as:

$$Re_x=\left(\frac{r^2\Omega}{\upsilon(1-bt)}\right).$$

4. Exploration of entropy generation

Within the influences of electric and magnetic forces, the phrase for volumetric entropy generation number is given as follows [15,16,26,27]:

$$S_{gen}''' = \frac{k_{hnf}}{T_0^2}\left[\left(\frac{\partial T}{\partial z}\right)^2 + \frac{16\sigma^* {T_0}^3}{3k^* k_{hnf}}\left(\frac{\partial T}{\partial z}\right)^2\right] + \frac{\mu_{hnf}}{T_0}\left[\left(\frac{\partial u}{\partial z}\right)^2 + \left(\frac{\partial v}{\partial z}\right)^2\right] + \frac{\sigma_{hnf}}{T_0(1-bt)}[E_0^2 + B_0^2(u^2+v^2)]. \quad (19)$$

The conduction, viscosity, and joule effects are all included in the above equation. The first term in the above formula exhibits irreversibility through heat conduction. The irreversibility produced by frictional effects is represented by the second term and the corresponding joule dissipation involving the magnetic and electric fields is represented by the third term. The entropy generation number can be stated as the dimensionless counterpart of the entropy generation rate, which is the ratio of the actual and characteristic entropy generation rates. So, the reduced entropy generation number equation can be written as follows:

$$N_G = \alpha_1\left\{N_4 + \frac{4}{3}Rd(1+\theta(\theta_w-1))^3\right\}\theta'^2 + N_1 Br(f''^2 + g'^2) + N_2 MBr\{E_1^2 + f'^2 + g^2\}. \quad (20)$$

Here, the dimensionless parameters are given below:

$$N_G = \frac{T_0 S_{gen}''' v(1-bt)}{k_f \Omega \Delta T}, \quad \Delta T = (T_s - T_0), \quad \alpha_1 = \frac{\Delta T}{T_0},$$

$$Br = \frac{\mu_f r^2 \Omega^2}{k_f (T_s - T_0)(1-bt)^2}.$$

But the entropy generation number is inadequate to overcome the difficulty like, the dominance of irreversibility mechanisms which is physically significant. To comprehend entropy generation methods, the Bejan number is used, which is the ratio of entropy generation owing to heat transfer to overall entropy generation.

$$Be = \frac{\alpha_1\left\{N_4 + \frac{4}{3}Rd(1+\theta(\theta_w-1))^3\right\}\theta'^2}{\alpha_1\left\{N_4 + \frac{4}{3}Rd(1+\theta(\theta_w-1))^3\right\}\theta'^2 + N_1 Br(f''^2 + g'^2)}. \quad (21)$$

Table 1 values and the quantities are used to get the output of the program in MATLAB. The hybrid nanofluid quantities are defined as:

Dynamic viscosity

$$\mu_{hnf} = \frac{\mu_f}{(1-\phi_{Ta})^{2.5}(1-\phi_{Co})^{2.5}}, \quad (22)$$

Density:

$$\rho_{hnf} = \rho_f(1-\phi_{Co})\left[(1-\phi_{Ta}) + \phi_{Ta}\left(\frac{\rho_{Ta}}{\rho_f}\right)\right] + \phi_{Co}(\rho_{Co}). \quad (23)$$

Heat capacity

$$(\rho c_p)_{hnf} = (\rho c_p)_f(1-\phi_{Co})(1-\phi_{Ta}) + \phi_{Ta}(\rho c_p)_{Ta} + \phi_{Co}(\rho c_p)_{Co}\ . \quad (24)$$

Table 1. Thermophysical properties of hybrid nanofluid.

Physical properties	Blood	Tantalum (*Ta*)	Cobalt (*Co*)
ρ $(\mathrm{kgm^{-3}})$	3617	16650	8900
$C_p(\mathrm{J(kg)^{-1}K^{-1}})$	1050	140	445
k $(\mathrm{W(m^{-1}K^{-1})})$	0.52	57	100
σ $(\Omega\mathrm{m})^{-1}$	1.33	7.7×10^6	1.7×10^7
Pr	21		

Electrical conductivity

$$\frac{\sigma_{hnf}}{\sigma_{bf}} = \left(\frac{(1+2\phi_{Co})\sigma_{Co} + 2(1-\phi_{Co})\sigma_{bf}}{(1-\phi_{Co})\sigma_{Co} + (2+\phi_{Co})\sigma_{bf}}\right), \quad (25)$$

where, $\frac{\sigma_{bf}}{\sigma_f} = \left(\frac{(1+2\phi_{Ta})\sigma_{Ta}+2(1-\phi_{Ta})\sigma_f}{(1-\phi_{Ta})\sigma_{Ta}+(2+\phi_{Ta})\sigma_f}\right)$.

Thermal conductivity

$$\frac{k_{hnf}}{k_{bf}} = \left(\frac{(1+2\phi_{Co})k_{Co} + 2(1-\phi_{Co})k_{bf}}{(1-\phi_{Co})k_{Co} + (2+\phi_{Co})k_{bf}}\right), \quad (26)$$

where, $\frac{k_{bf}}{k_f} = \left(\frac{(1+2\phi_{Ta})k_{Ta}+2(1-\phi_{Ta})k_f}{(1-\phi_{Ta})k_{Ta}+(2+\phi_{Ta})k_f}\right)$.

5. Method of solution

5.1. Runge-Kutta (RK) 4th order method

A boundary value issue is formed by Eqs. (9)-(11) and the boundary conditions of Eq. (12). Entropy generation Eq. (20) and Bejan number Eq. (21) are also converted as a result of this. The shooting technique is used to solve these equations by transforming them to an initial value problem. For this, we convert the above-mentioned non-linear ordinary differential equations to a system of first-order differential equations as follows:

$$f = \wp_1,\ f' = \wp_2,\ f'' = \wp_3,\ f''' = \wp_4,\ f^{iv} = \wp_4',\ g = \wp_5,$$
$$g' = \wp_6,\ g'' = \wp_6',\ \theta = \wp_8,\ \theta' = \wp_9,\ \theta'' = \wp_9'.$$

$$\wp_4' = \frac{\begin{bmatrix} 2(n_1/n_3)\beta_2\wp_3^2 - \beta_1(4\wp_1\wp_5\wp_6 + 4\wp_1^2\wp_4 \\ -4\wp_1\wp_2\wp_3) + (n_1/n_3)\wp_4 + (n_2/n_3)M(E_1-\wp_2) \\ -(n_1/n_3)\beta\wp_2 - S(\wp_2 + (\eta/2)\wp_3 \\ +(\wp_5^2 + 2\wp_1\wp_3 - \wp_2^2) \end{bmatrix}}{2\left(\frac{n_1}{n_3}\right)\beta_2\wp_1}, \quad (27)$$

$$\wp_7' = \frac{\begin{bmatrix} 2(n_1/n_3)\beta_2\wp_3\wp_6 - \beta_1(4\wp_2^2\wp_5 + 4\wp_1^2\wp_7 \\ -4\wp_1\wp_2\wp_6 - 4\wp_1\wp_3\wp_5) + (n_1/n_3)\wp_7 \\ +(n_2/n_3)M(E_1-\wp_5) - (n_1/n_3)\beta\wp_5 \\ -S[(\eta/2)\wp_6 + \wp_5] - 2(\wp_2\wp_5 - \wp_6\wp_1) \end{bmatrix}}{2\left(\frac{n_1}{n_3}\right)\beta_2\wp_1}, \quad (28)$$

$$\wp_9{}' = -\frac{\begin{bmatrix}(4/3)(Rd/n_5)[(Tw-1)^3(3\wp_8^2\wp_9^2)+3(Tw-1)^2\\ (2\wp_8\wp_9^2)+3(Tw-1)(\wp_9^2)]+(n_1/n_5)Ec\,Pr(\wp_3^2+\wp_6^2)\\ +2\,Pr(\wp_1\wp_9-\wp_8\wp_2)-S\,Pr[(3/2)\wp_8+(\eta/2)\wp_9]\\ +(Pr/n_5)QeExp(-n\xi)+(Pr/n_5)Qt\wp_8\\ +(n_2/n_5)MEc\,Pr(\wp_2^2+\wp_5^2+E_1^2)\end{bmatrix}}{\begin{matrix}(n_4/n_5)+(Rd/n_5)(4/3)[1+(Tw-1)^3\wp_8^3\\ +3(Tw-1)^2\wp_8^2+3(Tw-1)\wp_8]\end{matrix}}. \quad (29)$$

Now the boundary conditions as:

$$\wp_1(0)=0,\ \wp_2(0)=\omega,\ \wp_5(0)=1,\ \wp_8(0)=1,$$
$$\wp_2(\infty)=0,\ \wp_3(\infty)=0,\ \wp_5(\infty)=0,\ \wp_6(\infty)=0,$$
$$\wp_8(\infty)=0. \quad (30)$$

Followed by the entropy generation and Bejan number as shown below:

$$N_G=\alpha_1\{n_4+(4/3)(Rd)[1+\wp_8(Tw-1)]^3\}\wp_9^2 +n_1Br(\wp_3^2+\wp_6^2)+n_2MBr(E_1^2+\wp_2^2+\wp_5^2), \quad (31)$$

$$Be=\frac{\alpha_1\{n_4+(4/3)(Rd)[1+\wp_8(Tw-1)]^3\}\wp_9^2}{\begin{matrix}\alpha_1\{n_4+(4/3)(Rd)[1+\wp_8(Tw-1)]^3\}\wp_9^2\\ +n_1Br(\wp_3^2+\wp_6^2)+n_2MBr(E_1^2+\wp_2^2+\wp_5^2)\end{matrix}}. \quad (32)$$

The values of $\wp_4(0)$, $\wp_7(0)$ and $\wp_9(0)$ i.e., $f'''(0)$, $g''(0)$ and $\theta'(0)$ is required to integrate Eqs. (27) – (29) as an initial value problem, but such kind of values are not furnished at the boundary. So, the appropriate guess values are picked and then the integration process is performed. The selection of a suitable finite value of η at $\infty$is the most critical aspect of the shooting procedure. To find η at ∞ for the boundary value issue, we start with some initial estimate values for a certain set of physical parameters, culminating in obtain $f'''(0)$, $g''(0)$, and $\theta'(0)$. The operation is repeated with another enormous values of η at ∞ until two consecutive values of $f'''(0)$, $g''(0)$, and $\theta'(0)$ differ only by one significant digit. The most acceptable value of the limit η at ∞ for that specific collection of parameters is eventually chosen as the last value of η at ∞. For a different set of physical factors, the value of η at ∞may change. The integration begins once the finite value of η at ∞ has been determined. Adjust the estimated values f''', g'' and θ' to offer a better approximation to the solution by comparing the computed values for f', g and θ at $\eta = 8$ (say) with the specified boundary conditions $f'(8)=0$, $g(8)=0$ and $\theta(8)=0$. We use the fourth order Runge-Kutta technique with a step size of h = 0.01 to apply the series values for $f'''(0)$, $g''(0)$, $\theta'(0)$. The technique is continued until the findings have converged to the required degree of accuracy of 10^{-8}.

Through this method the values of skin friction coefficients and Nusselt number for different parameters like M, β_1, β_2, E_1, Rd, Ec, Pr, S, Q, Br and α_1 is dragged and then ANN is used for comparison and as well as to plot the output. Table 2 gives the comparison of $f'(0)$ for rotation parameter in R-K 4th order method which is performed in the MATLAB.

Table 2. Comparision of $f'(0)$ for various values of ω.

Variation of ω	Uddin et al. [28]	Mustafa et al. [29]	Ahmed et al. [30]	Present paper
0	-1.1740	-1.1737	-1.1739	-1.1734
1	-0.9485	-0.9483	-0.9484	-0.9488
2	-3265	-3263	-3264	-3248
-5	3.1939	3.1937	3.1937	3.5674
10	12.7211	12.7206	12.7209	12.7642
20	40.9059	40.9056	40.9057	40.89990

5.2.1. Artificial Neural Network (MLP-NN)

ANNs are built in the same way that human and animal brains are built. Basic scalar messages, simple processing components, a high degree of interconnection and adoptive interaction between units are the things which make them a type of multi-processor computer system [31]. Actually, ANN provides a reasonably quick and flexible way of modelling, so it is appropriate for rainfall-runoff prediction [32,33]. Layers of neurons make up an ANN. One or more hidden layers of neurons connect the input layer of neurons to the output layer of neurons. The interconnecting link between the neuron layers is made up of connection weights. This method changes its weights throughout the training phase to reduce the errors between the projected result and the actual output using the Back Propagation algorithm [34]. To get the best topology and weights, ANN is trained using experimental data and then evaluated with more experimental data whereas, bias refers to the weight that is provided directly to one neuron without being coupled to the prior neuron in specific circumstances. The most common type of ANN is the multilayer perceptron (MLP). It also has one or more hidden layers feed forward neural network. The sigmoid function was chosen as the activation function.

$$f(s)=\frac{1}{1+e^{-s}}, \quad (33)$$

where, $s_i=\sum_{i=1}^{n} W_i x_i$, in which the term W_i is related to weights and x_i for input values. In the next part, we'll go through the ANN implementation in more detail as we go over the learning methods.

5.2.2. Levenberg Marquardt Algorithm (LM-NN)

Levenberg Marquardt is the first learning algorithm to be implemented. LM is a fast-converging training technique that has a lot of applications in neural network discipline [35]. It's a variant of the standard Newton algorithm for determining the optimum answer to a minimization issue [36].

Two-layered neural networks with specific variables and parameters are shown in Figure 2. Here, indication of P_n is for input, $W_{(i,j)}$ for the first layer's connecting weight, $V_{(i.j)}$ for the second layer's connecting weight, and q_n for the output.

$$a(i)=\sum_{i=1}^{n} W_{(i,j)}P_i, \quad (34)$$

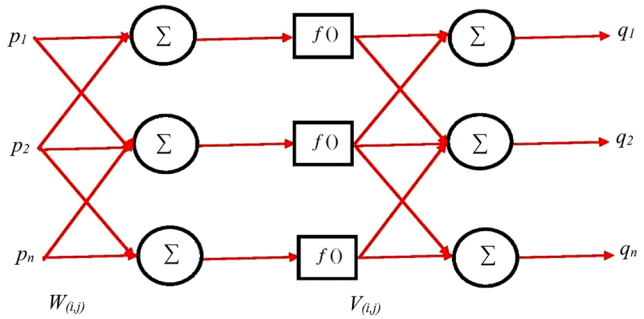

Figure 2. Neural network with two-layered hidden neuron.

The second layer's net output from unit i is as follows:

$$q(i) = \sum_{i=1}^{n} f\big(a(h)\big)V_{(i,j)}. \quad (35)$$

The goal of ANN is to figure out how input and output pairs are connected. The hidden unit is named as h , and the activation function is as $f()$. The Sigmoid function was chosen as the activation function.

$$f(s) = \frac{1}{1+e^{-s}}. \quad (36)$$

The Gauss-Newton technique provides an update.

$$\Delta x = [J^T(x)J(x)]^{-1}J^T(x)e(x), \quad (37)$$

while Levenberg Marquardt's to the Gauss-Newton technique is such that:

$$\Delta x = [J^T(x)J(x) + \mu I]^{-1}J^T(x)e(x). \quad (38)$$

When the scalar μ is 0, Eq. (38) is just Newton's technique; however, when the scalar μ is large, Eq. (33) becomes gradient descent with a short step size. The original description of Levenberg-Marquardt is explained in [37].

By incorporating information as input and calculating outputs, from different node activations and interconnection weights, this is how the output of ANN was calculated through the LM-NN method. The mean percentile error was computed after comparing the output to the experimental output. The error value was then transmitted backwards through the network and the weights at each node in each layer were adjusted accordingly. The method was then performed iteratively until the total error value fell below a predefined threshold. As shown in Figure 3, the eleven parameters (M,β_1,β_2,E_1,Rd,Ec,Pr,S,Q,Br, and α_1) that were obtained for the samples utilized in the research were used as input nodes, and three parameters (skin friction coefficients in xz and yz directions and Nusselt number) of these samples were employed as the ANN's output parameters. The method was then performed iteratively until the total error value fell below a predefined threshold. The numerical values acquired for all of the parameters in R-K 4th order method as shown in Tables 3, 4, and 5 were utilized to train the ANN in this research. Also, the following flow chart Figure 4, gives the sketch of how the output extraction is done through two methods. MPE value for this rate of heat trnasfer is (0.0034). MPE means mean

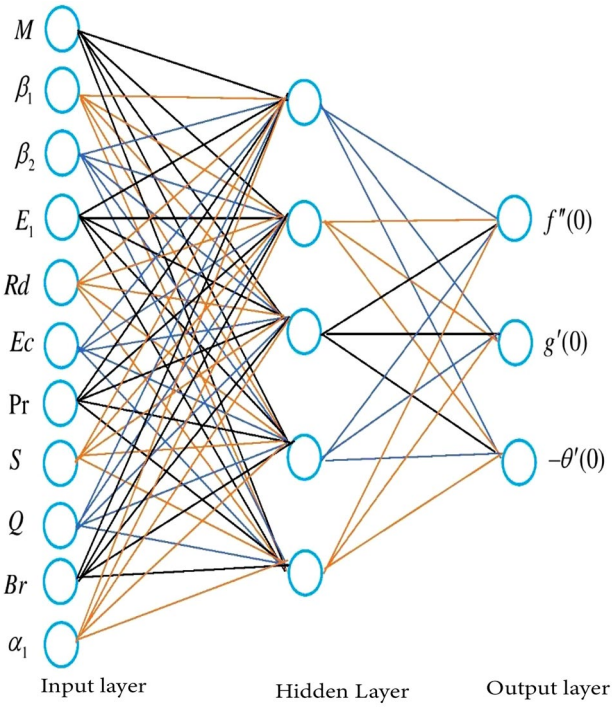

Figure 3. Schematic diagram of a multi-layer Artificial Neural Network (ANN).

percentile error for the $Cf_r\,Re_x^{1/2}$ is (0.9787) and for the $Cg_r\,Re_x^{1/2}$ is (0.9337).

6. Results and discussion

Numerical consequences performed for skin friction along x and y directions and Nusselt number are illustrated in this section through MATLAB and then ANN method of Levenberg Marquardt is used to compare the results. Also, the graphs of this parameters are performed by using ANN method. In MATLAB the results are gained for the accompanying fixed parametric values: $S = 0.3$, $M = 0.5$, $\beta_1 = 0.3$, $\beta_2 = 0.3$, $E_1 = 0.5$, $Rd = 1.0$, $Ec = 0.05$, $Q = 0.3$, $\alpha = 0.2$, and $Q_t = 0.2$. Actually, LM-NN is divided into three phases: training, validation, and testing. The activation function of artificial neurons was a sigmoid function and training was completed with a predetermined 176 number of epochs. The ANN model for the skin friction coefficients and Nusselt number was trained, validated and tested using a total of 44 numerical results. The training set consisted of 34 data sets, while the validation set consisted of 7 data sets and the balance of the data was utilised to evaluate the model's findings. Figures 5 and 6 show the skin friction coefficient of $Cf_r\,Re_x^{1/2}$ and $Cg_r\,Re_x^{1/2}$ whereas Figure 7 explores the Nusselt number for the proposed ANN model's training, validation, and test sets, respectively. This section shows the numerical results of skin friction coefficients ($Cf_r\,Re_x^{1/2}$ and $Cg_r\,Re_x^{1/2}$), as well as the Nusselt number ($Nu_x\,Re_x^{-1/2}$).

For all data sets, the model's MPE values were 0.9787, 0.9337, and 0.0034, respectively. Because they replicate complex relationships between input and output variables, the ANN models seem to have been effectively trained. Furthermore, the projected skin friction coefficients and

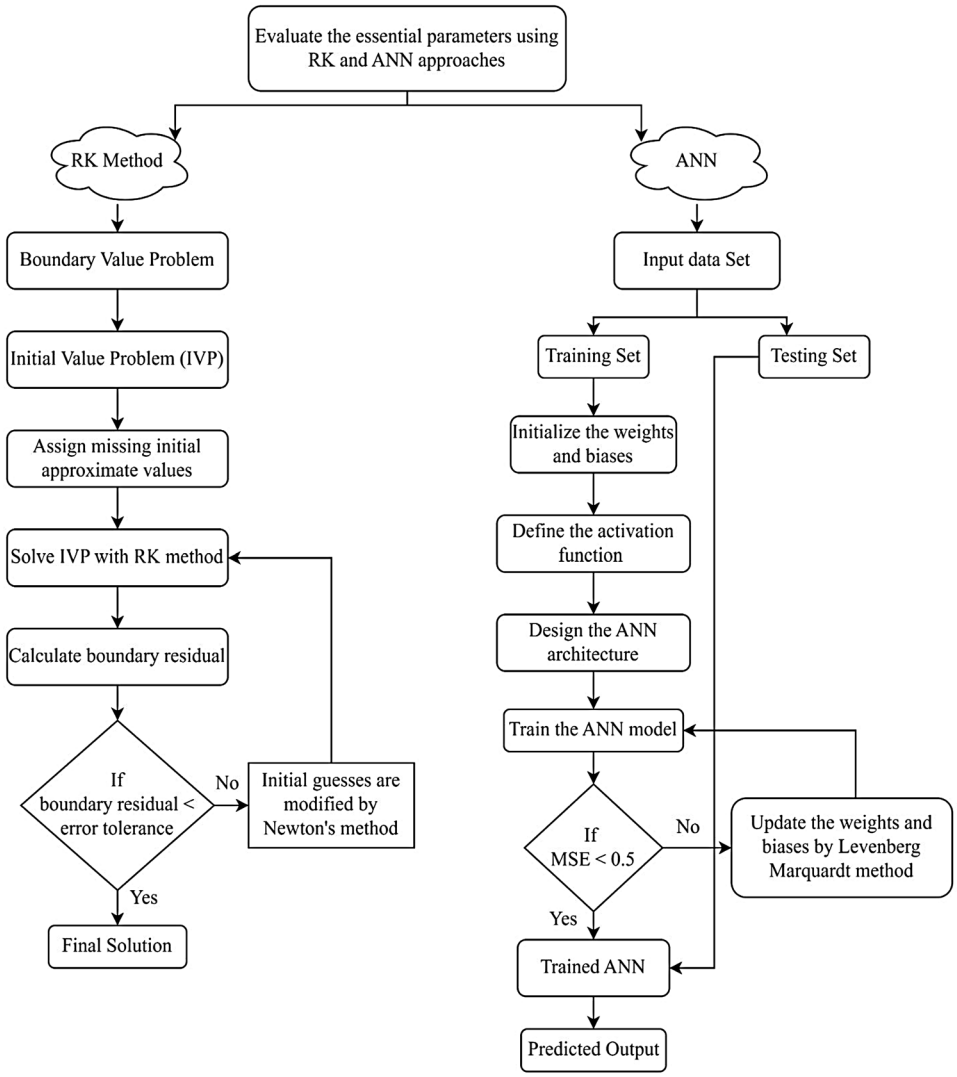

Figure 4. Flow chart representation for the extraction of outputs.

Nusselt number values from the ANN model are compared to numerically obtained skin friction coefficients and Nusselt number values for the training, validation, and test sets, as shown in Figures 5, 6, and 7 respectively. The ANN model's conclusions are quite similar to the numerical results. So far, our study has proven that the ANN can accurately simulate skin friction coefficients and the Nusselt number. The numerical findings and the ANN (LM-NN) model's conclusions are very comparable.

From the Figure 8, it is noticed that for the higher values of Eckert number and radiation parameters, the skin friction coefficient $Cf_r\, Re_x^{1/2}$ will decline automatically. Similarly, when the Brinkman number and temperature ratio parameter intensify, $Cf_r\, Re_x^{1/2}$ decreases, as seen in Figure 9. It is evident that from the Figure 10, that skin friction coefficient $Cf_r\, Re_x^{1/2}$ declines for the higher values of the parameters Q and Pr. Figure 11 shows the decreasing tendency of $Cg_r\, Re_x^{1/2}$ for increasing parameters Brinkman number and temperature ratio parameter. Also, $Cg_r\, Re_x^{1/2}$ declines for the higher values of the parameters Q and Pr which is illustrated in the Figure 12.

Figure 13 demonstrates that for the higher values of electric field and unsteady parameters is observed to be inclined for the rate of heat transfer $Nu_x\, Re_x^{-1/2}$. For the parameter values of Deborah number and magnetic field on Nusselt number is explored in the Figure 14. But it is seen from the Figure 13 that for those parameters Nusselt number $Nu_x\, Re_x^{-1/2}$ declines as those parameters increases.

From the MATLAB, Figures 15-18 is extracted on entropy generation parameter. Figure 15 shows how the entropy generation intensifies as the magnetic field strength increases. Physically, increasing the Lorentz force by increasing the magnetic parameter creates greater friction, which increases the rate of entropy generation. As seen in Figure 16, the entropy production rate reduces as the electric field intensity increases. Figure 17 shows that the entropy production rate increases as the Brinkman number increases. Because viscous effects have gotten greater with the growth in Brinkman numbers, this condition in the entropy generating rate outcomes has arisen. The entropy generation rises for the greater values of the temperature ratio parameter is observed from Figure 18.

Table 3. The results of skin friction coefficient in *xz*-direction ($Cf_r\, Re_x^{\frac{1}{2}}$) for variation of non-dimensional parameters in NM and ANN methods.

M	β_1	β_2	E_1	Rd	Ec	Pr	S	Q	Br	α_1	$Cf_r Re_x^{1/2}$	
											NM	**ANN**
0.4	0.3	0.3	0.5	1	0.05	21	0.3	0.5	1	0.5	0.180954	0.175389505
1	0.3	0.3	0.5	1	0.05	21	0.3	0.5	1	0.5	0.126905	0.303769159
1.5	0.3	0.3	0.5	1	0.05	21	0.3	0.5	1	0.5	0.412864	0.462084033
2	0.3	0.3	0.5	1	0.05	21	0.3	0.5	1	0.5	0.656983	0.638455915
0.5	0.5	0.3	0.5	1	0.05	21	0.3	0.5	1	0.5	0.589509	0.561950011
0.5	0.7	0.3	0.5	1	0.05	21	0.3	0.5	1	0.5	0.828792	0.818177984
0.5	0.9	0.3	0.5	1	0.05	21	0.3	0.5	1	0.5	0.960801	0.970471947
0.5	1	0.3	0.5	1	0.05	21	0.3	0.5	1	0.5	1.011441	1.03990803
0.5	0.3	0.5	0.5	1	0.05	21	0.3	0.5	1	0.5	0.092991	0.097209999
0.5	0.3	0.7	0.5	1	0.05	21	0.3	0.5	1	0.5	0.005273	0.021628322
0.5	0.3	0.9	0.5	1	0.05	21	0.3	0.5	1	0.5	0.10714	0.047722595
0.5	0.3	1	0.5	1	0.05	21	0.3	0.5	1	0.5	0.15458	0.083779202
0.5	0.3	0.3	1	1	0.05	21	0.3	0.5	1	0.5	0.503506	0.474899651
0.5	0.3	0.3	1.5	1	0.05	21	0.3	0.5	1	0.5	0.791431	0.778354012
0.5	0.3	0.3	2	1	0.05	21	0.3	0.5	1	0.5	1.058272	1.069551658
0.5	0.3	0.3	2.5	1	0.05	21	0.3	0.5	1	0.5	1.310675	1.361511662
0.5	0.3	0.3	0.5	1.01	0.05	21	0.3	0.5	1	0.5	0.180955	0.181336731
0.5	0.3	0.3	0.5	1.02	0.05	21	0.3	0.5	1	0.5	0.180955	0.174620691
0.5	0.3	0.3	0.5	1.03	0.05	21	0.3	0.5	1	0.5	0.180955	0.173013873
0.5	0.3	0.3	0.5	1.04	0.05	21	0.3	0.5	1	0.5	0.180952	0.177641111
0.5	0.3	0.3	0.5	1	0.06	21	0.3	0.5	1	0.5	0.180955	0.062545074
0.5	0.3	0.3	0.5	1	0.07	21	0.3	0.5	1	0.5	0.180955	0.060015182
0.5	0.3	0.3	0.5	1	0.075	21	0.3	0.5	1	0.5	0.180955	0.108829085
0.5	0.3	0.3	0.5	1	0.08	21	0.3	0.5	1	0.5	0.180926	0.195774692
0.5	0.3	0.3	0.5	1	0.05	22	0.3	0.5	1	0.5	0.180955	0.17040481
0.5	0.3	0.3	0.5	1	0.05	23	0.3	0.5	1	0.5	0.180955	0.153384096
0.5	0.3	0.3	0.5	1	0.05	24	0.3	0.5	1	0.5	0.180957	0.142748524
0.5	0.3	0.3	0.5	1	0.05	25	0.3	0.5	1	0.5	0.180955	0.139546792
0.5	0.3	0.3	0.5	1	0.05	21	0.4	0.5	1	0.5	0.059617	0.071292267
0.5	0.3	0.3	0.5	1	0.05	21	0.5	0.5	1	0.5	0.061644	0.065388207
0.5	0.3	0.3	0.5	1	0.05	21	0.6	0.5	1	0.5	0.182646	0.188357507
0.5	0.3	0.3	0.5	1	0.05	21	0.7	0.5	1	0.5	0.879077	0.462949872
0.5	0.3	0.3	0.5	1	0.05	21	0.3	0.6	1	0.5	0.180955	0.177856431
0.5	0.3	0.3	0.5	1	0.05	21	0.3	0.7	1	0.5	0.180954	0.173303424
0.5	0.3	0.3	0.5	1	0.05	21	0.3	0.8	1	0.5	0.180955	0.173649336
0.5	0.3	0.3	0.5	1	0.05	21	0.3	0.9	1	0.5	0.180951	0.176309007
0.5	0.3	0.3	0.5	1	0.05	21	0.3	0.5	2	0.5	0.180954	0.157172958
0.5	0.3	0.3	0.5	1	0.05	21	0.3	0.5	3	0.5	0.180955	0.140630514
0.5	0.3	0.3	0.5	1	0.05	21	0.3	0.5	4	0.5	0.180955	0.137576406
0.5	0.3	0.3	0.5	1	0.05	21	0.3	0.5	5	0.5	0.180956	0.140571371
0.5	0.3	0.3	0.5	1	0.05	21	0.3	0.5	1	1	0.180954	0.166158253
0.5	0.3	0.3	0.5	1	0.05	21	0.3	0.5	1	1.5	0.180955	0.151442347
0.5	0.3	0.3	0.5	1	0.05	21	0.3	0.5	1	2	0.180956	0.148057221
0.5	0.3	0.3	0.5	1	0.05	21	0.3	0.5	1	2.5	0.180957	0.152687531

Table 4. The results of skin friction coefficient in *yz*-direction ($Cg_r \mathrm{Re}_x^{1/2}$) for variation of non-dimensional parameters in NM and ANN methods.

M	β_1	β_2	E_1	Rd	Ec	Pr	S	Q	Br	α_1	$Cg_r Re_x^{1/2}$	
											NM	**ANN**
0.4	0.3	0.3	0.5	1	0.05	21	0.3	0.5	1	0.5	1.327998	1.340937
1	0.3	0.3	0.5	1	0.05	21	0.3	0.5	1	0.5	0.662449	0.638885
1.5	0.3	0.3	0.5	1	0.05	21	0.3	0.5	1	0.5	0.17261	0.254505
2	0.3	0.3	0.5	1	0.05	21	0.3	0.5	1	0.5	0.23152	0.223987
0.5	0.5	0.3	0.5	1	0.05	21	0.3	0.5	1	0.5	0.141119	0.487026
0.5	0.7	0.3	0.5	1	0.05	21	0.3	0.5	1	0.5	0.663203	0.670841
0.5	0.9	0.3	0.5	1	0.05	21	0.3	0.5	1	0.5	1.006453	1.007673
0.5	1	0.3	0.5	1	0.05	21	0.3	0.5	1	0.5	1.1494	1.155552
0.5	0.3	0.5	0.5	1	0.05	21	0.3	0.5	1	0.5	1.04852	1.055171
0.5	0.3	0.7	0.5	1	0.05	21	0.3	0.5	1	0.5	0.865893	0.872098
0.5	0.3	0.9	0.5	1	0.05	21	0.3	0.5	1	0.5	0.676538	0.683434
0.5	0.3	1	0.5	1	0.05	21	0.3	0.5	1	0.5	0.58649	0.588191
0.5	0.3	0.3	1	1	0.05	21	0.3	0.5	1	0.5	1.586397	1.56276
0.5	0.3	0.3	1.5	1	0.05	21	0.3	0.5	1	0.5	1.900585	1.880991
0.5	0.3	0.3	2	1	0.05	21	0.3	0.5	1	0.5	2.17816	2.168212
0.5	0.3	0.3	2.5	1	0.05	21	0.3	0.5	1	0.5	2.430464	2.417294
0.5	0.3	0.3	0.5	1.01	0.05	21	0.3	0.5	1	0.5	1.212865	1.226756
0.5	0.3	0.3	0.5	1.02	0.05	21	0.3	0.5	1	0.5	1.212864	1.206707
0.5	0.3	0.3	0.5	1.03	0.05	21	0.3	0.5	1	0.5	1.212865	1.189762
0.5	0.3	0.3	0.5	1.04	0.05	21	0.3	0.5	1	0.5	1.212862	1.197756
0.5	0.3	0.3	0.5	1	0.06	21	0.3	0.5	1	0.5	1.212865	1.224325
0.5	0.3	0.3	0.5	1	0.07	21	0.3	0.5	1	0.5	1.212867	1.213953
0.5	0.3	0.3	0.5	1	0.075	21	0.3	0.5	1	0.5	1.204971	1.212355
0.5	0.3	0.3	0.5	1	0.08	21	0.3	0.5	1	0.5	1.204972	1.21708
0.5	0.3	0.3	0.5	1	0.05	22	0.3	0.5	1	0.5	1.212865	1.212476
0.5	0.3	0.3	0.5	1	0.05	23	0.3	0.5	1	0.5	1.212863	1.213684
0.5	0.3	0.3	0.5	1	0.05	24	0.3	0.5	1	0.5	1.212866	1.218493
0.5	0.3	0.3	0.5	1	0.05	25	0.3	0.5	1	0.5	1.212865	1.217806
0.5	0.3	0.3	0.5	1	0.05	21	0.4	0.5	1	0.5	1.021271	1.081952
0.5	0.3	0.3	0.5	1	0.05	21	0.5	0.5	1	0.5	0.828563	0.916587
0.5	0.3	0.3	0.5	1	0.05	21	0.6	0.5	1	0.5	0.634841	0.61765
0.5	0.3	0.3	0.5	1	0.05	21	0.7	0.5	1	0.5	0.256313	0.254465
0.5	0.3	0.3	0.5	1	0.05	21	0.3	0.6	1	0.5	1.212865	1.221281
0.5	0.3	0.3	0.5	1	0.05	21	0.3	0.7	1	0.5	1.212866	1.209103
0.5	0.3	0.3	0.5	1	0.05	21	0.3	0.8	1	0.5	1.212867	1.210062
0.5	0.3	0.3	0.5	1	0.05	21	0.3	0.9	1	0.5	1.21286	1.215866
0.5	0.3	0.3	0.5	1	0.05	21	0.3	0.5	2	0.5	1.212864	1.207685
0.5	0.3	0.3	0.5	1	0.05	21	0.3	0.5	3	0.5	1.212865	1.210535
0.5	0.3	0.3	0.5	1	0.05	21	0.3	0.5	4	0.5	1.212866	1.207033
0.5	0.3	0.3	0.5	1	0.05	21	0.3	0.5	5	0.5	1.212866	1.213101
0.5	0.3	0.3	0.5	1	0.05	21	0.3	0.5	1	1	1.212864	1.229174
0.5	0.3	0.3	0.5	1	0.05	21	0.3	0.5	1	1.5	1.212865	1.218506
0.5	0.3	0.3	0.5	1	0.05	21	0.3	0.5	1	2	1.2128656	1.217304
0.5	0.3	0.3	0.5	1	0.05	21	0.3	0.5	1	2.5	1.212868	1.226123

Table. 5 The results of heat transfer coefficient (Nusselt number $Nu_x \mathrm{Re}_x^{-1/2}$) for variation of non-dimensional parameters in NM and ANN methods.

M	β_1	β_2	E_1	Rd	Ec	Pr	S	Q	Br	α_1	$Nu_x Re_x^{-1/2}$	
											NM	**ANN**
0.4	0.3	0.3	0.5	1	0.05	21	0.3	0.5	1	0.5	17.000741	16.82814
1	0.3	0.3	0.5	1	0.05	21	0.3	0.5	1	0.5	16.567447	16.48499
1.5	0.3	0.3	0.5	1	0.05	21	0.3	0.5	1	0.5	16.092525	16.08554
2	0.3	0.3	0.5	1	0.05	21	0.3	0.5	1	0.5	15.60204	15.59453
0.5	0.5	0.3	0.5	1	0.05	21	0.3	0.5	1	0.5	16.462047	16.34181
0.5	0.7	0.3	0.5	1	0.05	21	0.3	0.5	1	0.5	16.083963	16.03002
0.5	0.9	0.3	0.5	1	0.05	21	0.3	0.5	1	0.5	15.889186	15.85824
0.5	1	0.3	0.5	1	0.05	21	0.3	0.5	1	0.5	15.798502	15.76673
0.5	0.3	0.5	0.5	1	0.05	21	0.3	0.5	1	0.5	16.591513	16.56418
0.5	0.3	0.7	0.5	1	0.05	21	0.3	0.5	1	0.5	16.597923	16.53073
0.5	0.3	0.9	0.5	1	0.05	21	0.3	0.5	1	0.5	16.590622	16.59721
0.5	0.3	1	0.5	1	0.05	21	0.3	0.5	1	0.5	16.584462	16.57361
0.5	0.3	0.3	1	1	0.05	21	0.3	0.5	1	0.5	16.348064	16.33492
0.5	0.3	0.3	1.5	1	0.05	21	0.3	0.5	1	0.5	15.860596	15.79266
0.5	0.3	0.3	2	1	0.05	21	0.3	0.5	1	0.5	15.17239	15.1144
0.5	0.3	0.3	2.5	1	0.05	21	0.3	0.5	1	0.5	14.308991	14.30859
0.5	0.3	0.3	0.5	1.01	0.05	21	0.3	0.5	1	0.5	16.634018	16.71902
0.5	0.3	0.3	0.5	1.02	0.05	21	0.3	0.5	1	0.5	16.700332	16.69104
0.5	0.3	0.3	0.5	1.03	0.05	21	0.3	0.5	1	0.5	16.766395	16.72045
0.5	0.3	0.3	0.5	1.04	0.05	21	0.3	0.5	1	0.5	16.832208	16.81933
0.5	0.3	0.3	0.5	1	0.06	21	0.3	0.5	1	0.5	16.350909	16.41846
0.5	0.3	0.3	0.5	1	0.07	21	0.3	0.5	1	0.5	16.133422	16.13728
0.5	0.3	0.3	0.5	1	0.075	21	0.3	0.5	1	0.5	16.024311	16.01738
0.5	0.3	0.3	0.5	1	0.08	21	0.3	0.5	1	0.5	15.914968	15.9082
0.5	0.3	0.3	0.5	1	0.05	22	0.3	0.5	1	0.5	16.947166	16.94725
0.5	0.3	0.3	0.5	1	0.05	23	0.3	0.5	1	0.5	17.317468	17.17922
0.5	0.3	0.3	0.5	1	0.05	24	0.3	0.5	1	0.5	17.678965	17.58596
0.5	0.3	0.3	0.5	1	0.05	25	0.3	0.5	1	0.5	18.032213	18.03619
0.5	0.3	0.3	0.5	1	0.05	21	0.4	0.5	1	0.5	16.725507	16.71665
0.5	0.3	0.3	0.5	1	0.05	21	0.5	0.5	1	0.5	16.863043	16.69781
0.5	0.3	0.3	0.5	1	0.05	21	0.6	0.5	1	0.5	16.980051	16.82854
0.5	0.3	0.3	0.5	1	0.05	21	0.7	0.5	1	0.5	17.075629	17.06855
0.5	0.3	0.3	0.5	1	0.05	21	0.3	0.6	1	0.5	16.53894	16.63236
0.5	0.3	0.3	0.5	1	0.05	21	0.3	0.7	1	0.5	16.510421	16.50309
0.5	0.3	0.3	0.5	1	0.05	21	0.3	0.8	1	0.5	16.481884	16.43332
0.5	0.3	0.3	0.5	1	0.05	21	0.3	0.9	1	0.5	16.453333	16.44709
0.5	0.3	0.3	0.5	1	0.05	21	0.3	0.5	2	0.5	16.567447	16.57789
0.5	0.3	0.3	0.5	1	0.05	21	0.3	0.5	3	0.5	16.567447	16.50601
0.5	0.3	0.3	0.5	1	0.05	21	0.3	0.5	4	0.5	16.567447	16.56003
0.5	0.3	0.3	0.5	1	0.05	21	0.3	0.5	5	0.5	16.567447	16.54298
0.5	0.3	0.3	0.5	1	0.05	21	0.3	0.5	1	1	16.567447	16.82961
0.5	0.3	0.3	0.5	1	0.05	21	0.3	0.5	1	1.5	16.567447	16.74716
0.5	0.3	0.3	0.5	1	0.05	21	0.3	0.5	1	2	16.567447	16.56055
0.5	0.3	0.3	0.5	1	0.05	21	0.3	0.5	1	2.5	16.567447	16.35167

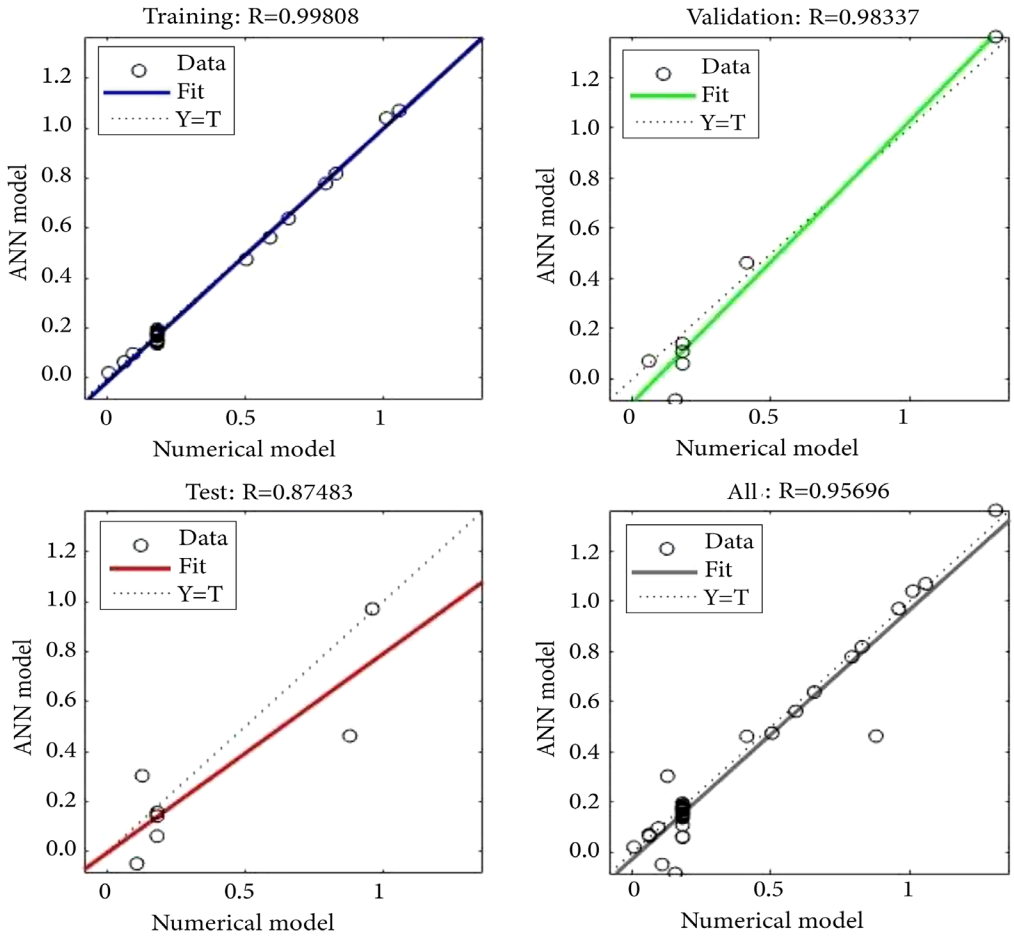

Figure 5. Graphical representation of the skin friction coefficient ($Cf_r\, Re_x^{1/2}$).

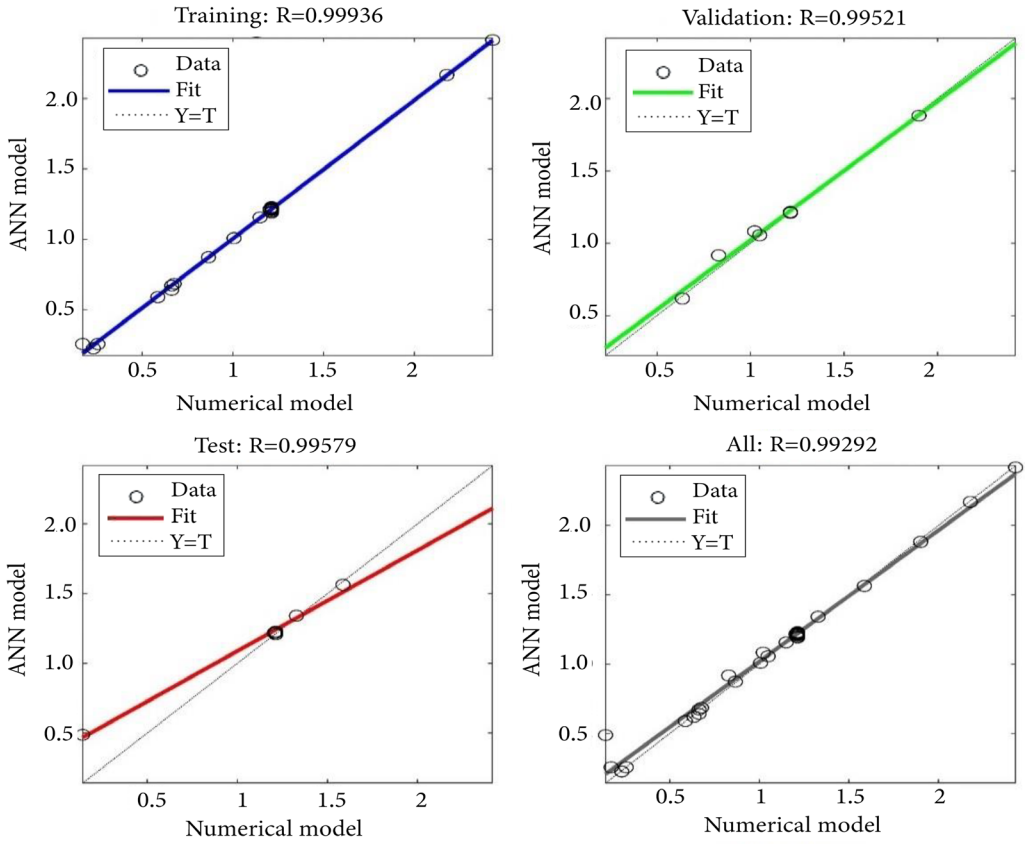

Figure 6. Graphical representation of the skin friction coefficient ($Cg_r\, Re_x^{1/2}$).

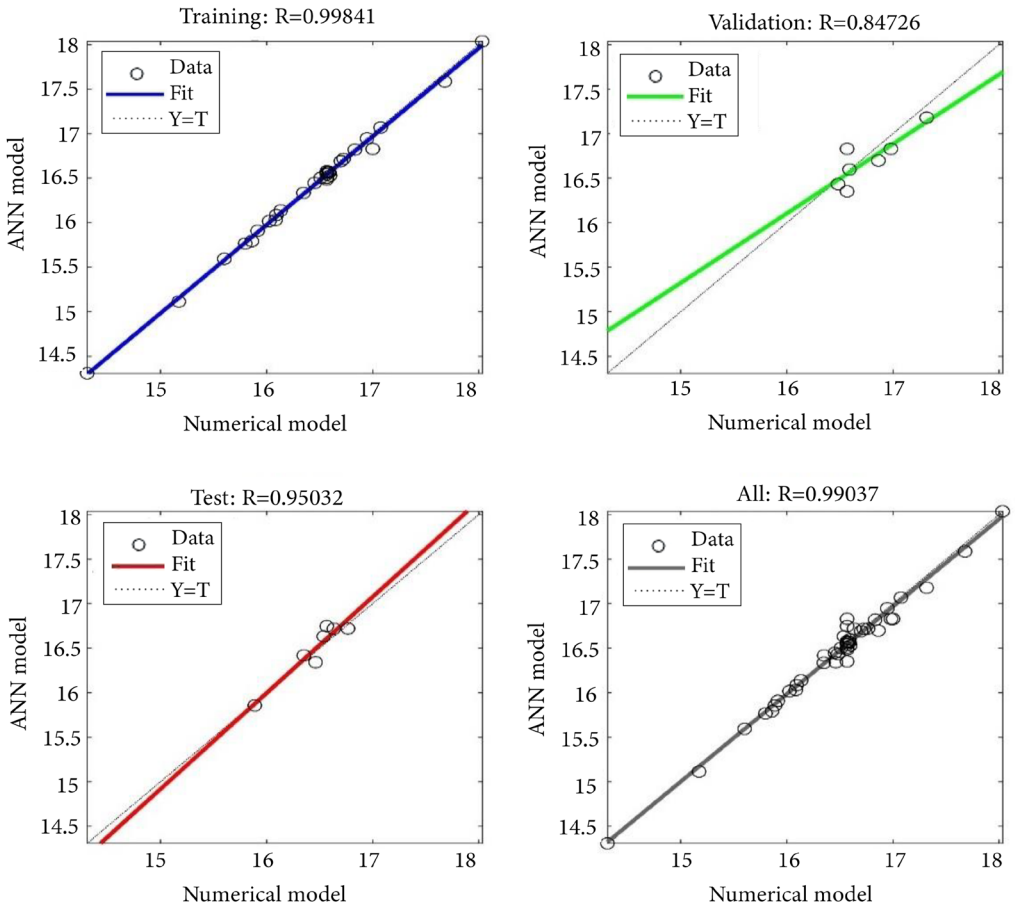

Figure 7. Graphical representation of the Nusselt number($Nu_x\, Re_x^{-1/2}$).

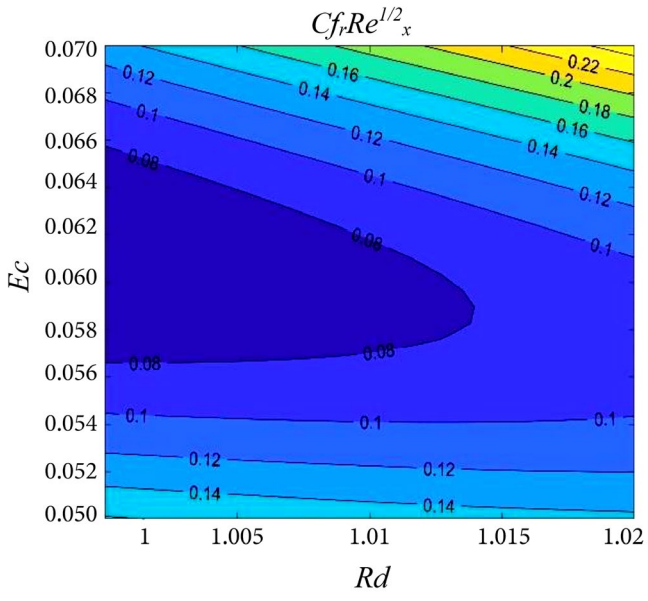

Figure 8. Sway of Ec and Rd on $Cf_r\, Re_x^{1/2}$

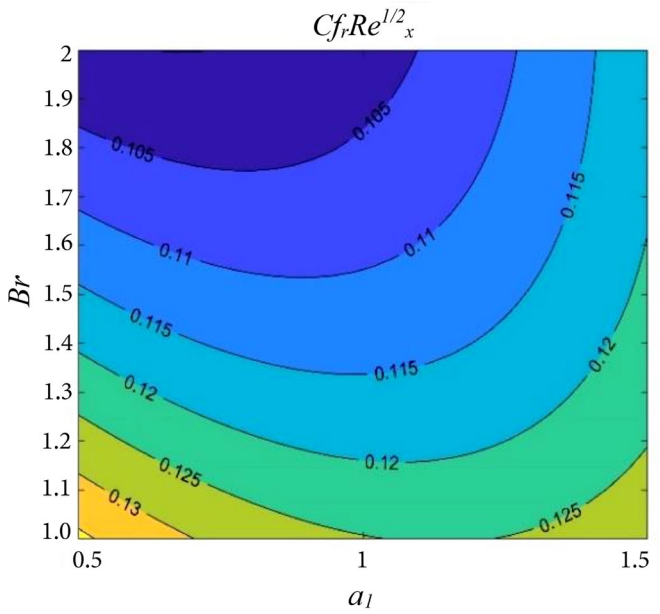

Figure 9. Sway of Br and α_1 on $Cf_r\, Re_x^{1/2}$.

7. Main findings

The numerical modelling and ANN(LM-NN) model results are quite close to the numerical findings. As a result of the present study's results, the suggested ANN model is successful for EMHD boundary layer slip flow over a rotating disk embedded in a porous medium with Oldroyd-B fluid. Also, PDEs are converted to ODEs using the relevant conversions. The reference set is generated using the R-K 4th order approach with the shooting methodology and then generated by using ANN(LM-NN) method for varying relevant parameters values. The major output drawn from this study can be summarized as below:

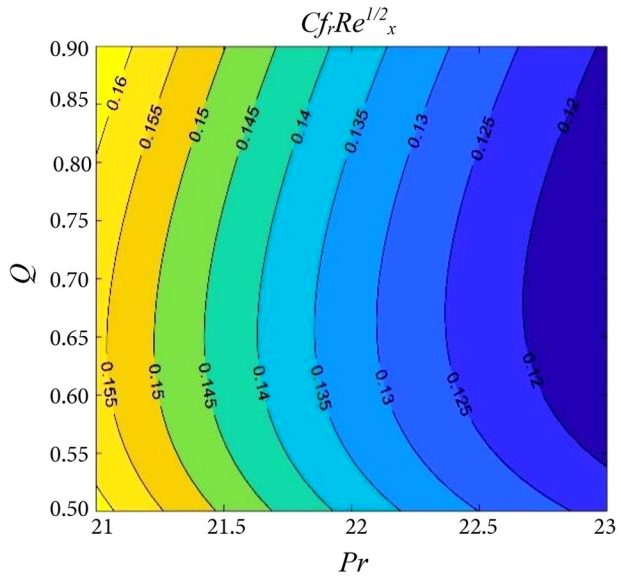

Figure 10. Sway of Q and Pr on $Cf_r\, Re_x^{1/2}$.

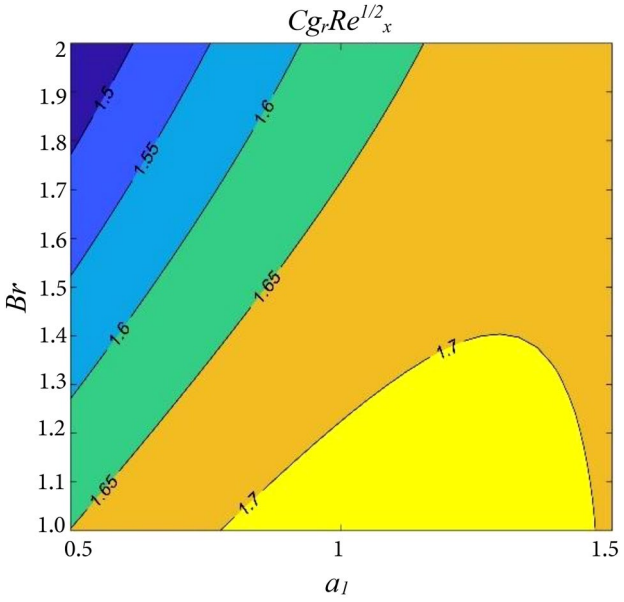

Figure 11. Sway of Br and α_1 on $Cg_r\, Re_x^{1/2}$.

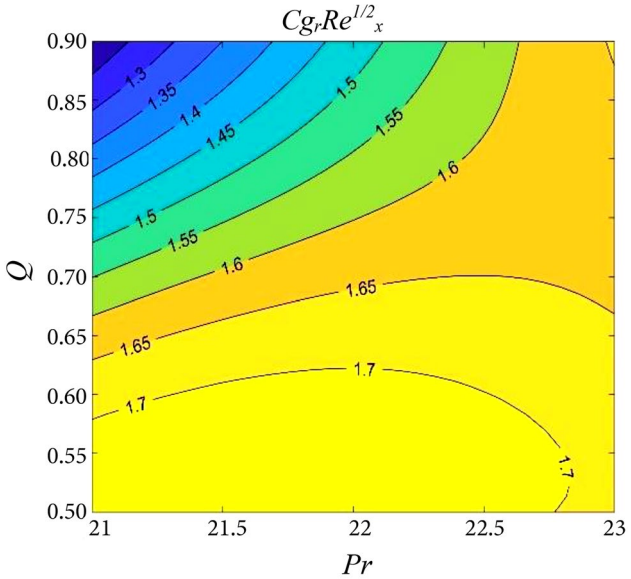

Figure 12. Sway of Q and Pr on $Cg_r\, Re_x^{1/2}$.

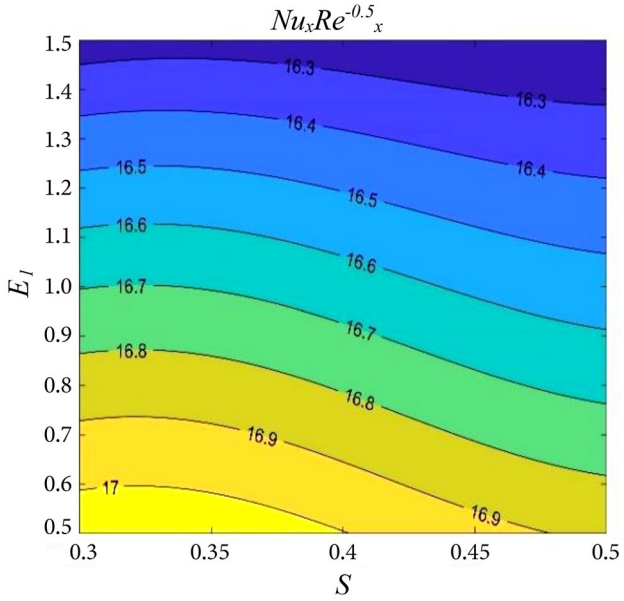

Figure 13. Sway of E_1 and S on $Nu_x\, Re_x^{-1/2}$.

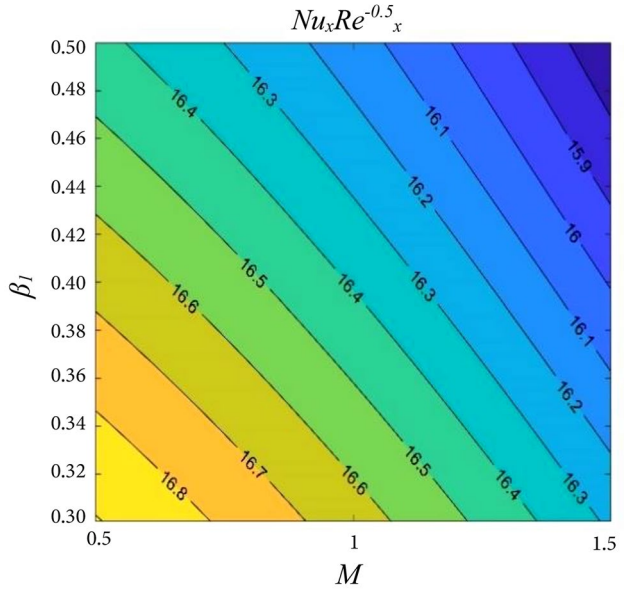

Figure 14. Sway of β_1 and M on $Nu_x\, Re_x^{-1/2}$.

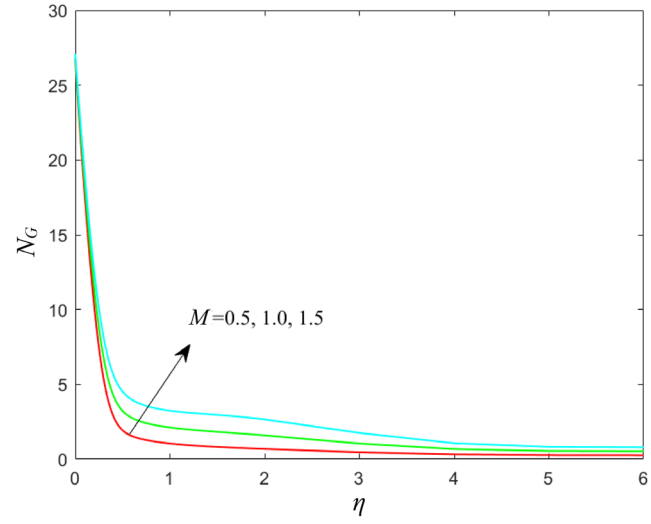

Figure 15. Sway of M on N_G.

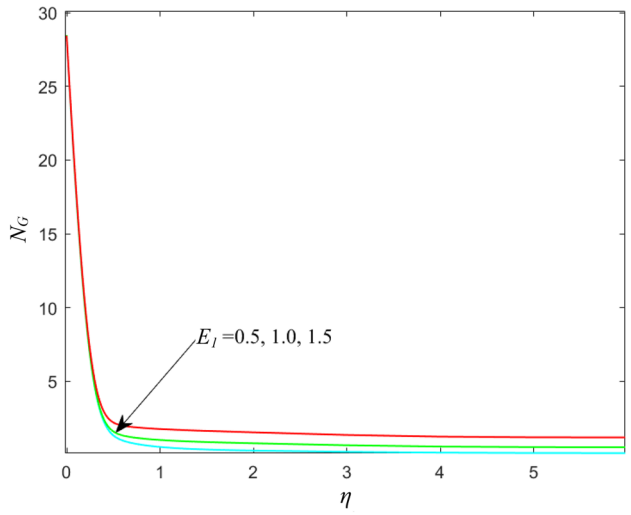

Figure 16. Sway of E_1 on N_G.

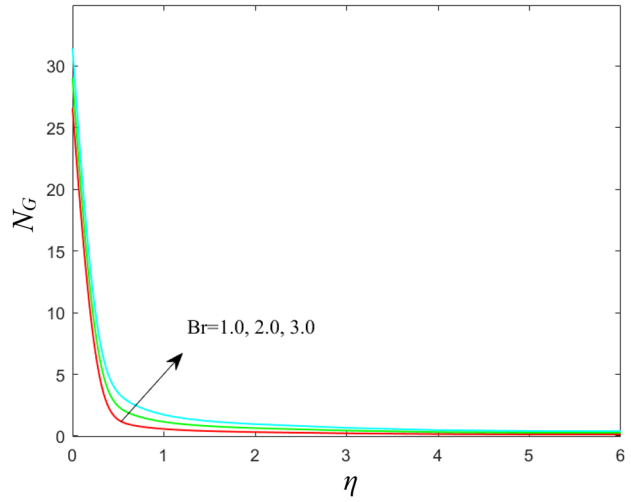

Figure 17. Sway of Br on N_G.

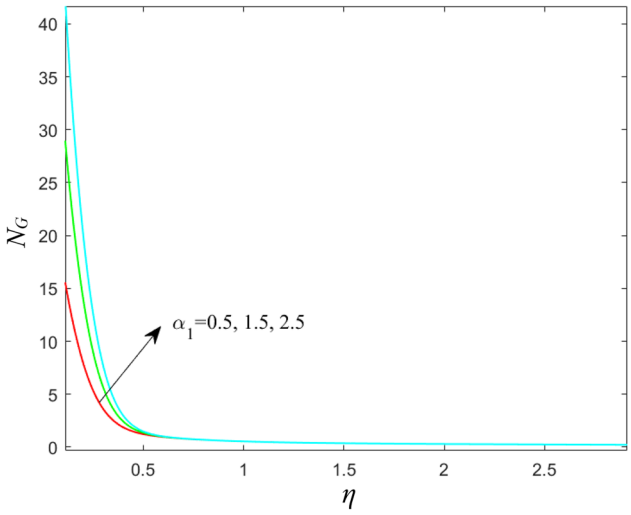

Figure 18. Sway of α_1 on N_G.

- Skin friction coefficients decrease for the higher values of Eckert number and radiation parameters;
- The rate of heat transfer declines for the rise in magnetic and Deborah number parameters;
- For the rise in the parameters like Brinkman number, Prandtl number and temperature ratio parameter, both the skin frictions will decline;
- Heat transfer increases with increasing in electric and unsteady parameters;
- Entropy generation rises for magnetic field, Brinkman number and temperature ratio parameter;
- Increase in the electric field parameter, entropy generation declines.

This current therapeutic model will be very interesting to clinicians for the treatment of anemia as well as in the treatment of microbial infections etc. Since we considered tantalum and cobalt as nanoparticles in which tantalum is utilized in bone implants and iodinated agents for blood imaging because of its longer circulation time. Cobalt is a component of vitamin B12, which stimulates red blood cell formation.

List of symbols

r, φ, z	Cylindrical coordinates
u, v, w	Velocity components
f	Axial velocity field
f'	Radial velocity field
g	Azimuthal velocity field
T	Temperature of the fluid
S	Measure of unsteadiness
M	Magnetic field parameter
B_0	Uniform magnetic field
T_s	Surface temperature
T_0	Origin temperature
T_{ref}	Constant reference temperature
Re	Local Reynolds number
Ec	Eckert number
Pr	Prandtl number
Rd	Thermal radiation
N_G	Local entropy generation
$Cf_r\, Re_x^{1/2}$	Skin friction co-efficient of f velocity
$Cg_r\, Re_x^{1/2}$	Skin friction co-efficient of g velocity
$Nu_x\, Re_x^{-1/2}$	Local Nusselt number

Be	Bejan number
N_1, N_2, N_3, N_4, N_5	Hybrid nanofluid constants
k	Thermal conductivity
Q_T^*	Thermal-dependent heat source coefficient
Q_E^*	Exponential space-dependent heat source coefficient
n	Exponential index
c	Stretching rate
Q	Exponential based heat source parameter
Q_t	Thermal space dependent heat source parameter

Greek symbols

ρ	Fluid density
υ	kinematic viscosity
μ	Dynamic viscosity
σ	Electric conductivity
η	Dimensionless variable
k^*	Mean absorption co-efficient
σ^*	Stefan Boltzmann constant
θ	Dimensionless temperature
ϕ_{Ta}	Volume fraction of tantalum
ϕ_{Co}	Volume fraction of Cobalt
Ω	Angular velocity
λ_1	Relaxation time parameter
β	Porosity parameter
β_1, β_2	Deborah numbers
θ_w	Temperature ratio parameter
α_1	Temperature difference parameter
ω	Rotation parameter

Subscripts

f	Fluid
nf	Nanofluid
hnf	Hybrid nanofluid

Funding

This research did not receive any specific grant from funding agencies in the public, commercial, or not-for-profit sectors.

Conflicts of interest

The authors declare that they have no known competing financial interests or personal relationships that could have appeared to influence the work reported in this paper.

Authors contribution statement

Frist and second authors

Abbai Reddy Divya and Polu Bala Anki Reddy: Conceptualization; Methodology; Software, Writing – review & editing of this manuscript.

References

1. Abbas, S.Z., Khan, W.A., Waqas, M., et al. "Exploring the features for flow of Oldroyd-B liquid film subjected to rotating disk with homogeneous/heterogeneous processes", *Comput. Methods Programs Biomed.*, **189**, 105323 (2020). https://doi.org/10.1016/J.CMPB.2020.105323
2. Hafeez, A., Khan, M., and Ahmed, J. "Stagnation point flow of radiative Oldroyd-B nanofluid over a rotating disk", *Comput. Methods Programs Biomed.*, **191**, p. 105342 (2020). https://doi.org/10.1016/j.cmpb.2020.105342
3. Waqas, H., Imran, M., Muhammad, T., et al. "Numerical investigation on bioconvection flow of Oldroyd-B nanofluid with nonlinear thermal radiation and motile microorganisms over rotating disk", *J. Therm. Anal. Calorim. 2020 1452*, **145**(2), pp. 523–539 (2020). https://doi.org/10.1007/S10973-020-09728-2
4. Hafeez, A., Khan, M., and Ahmed, J. "Thermal aspects of chemically reactive Oldroyd-B fluid flow over a rotating disk with Cattaneo–Christov heat flux theory", *J. Therm. Anal. Calorim. 2020 1443*, **144**(3), pp. 793–803 (2020). https://doi.org/10.1007/S10973-020-09421-4
5. Oldroyd, J.G. "On the formulation of rheological equations of state", *Proc. R. Soc. London. Ser. A. Math. Phys. Sci.*, **200**(1063), pp. 523–541 (1950). https://doi.org/10.1098/RSPA.1950.0035
6. Wang, J., Ijaz Khan, M., Khan, W.A., et al. "Transportation of heat generation/absorption and radiative heat flux in homogeneous–heterogeneous catalytic reactions of non-Newtonian fluid (Oldroyd-B model)", *Comput. Methods Programs Biomed.*, **189**, p. 105310 (2020). https://doi.org/10.1016/J.CMPB.2019.105310
7. Khan, M., Hafeez, A., and Ahmed, J. "Impacts of non-linear radiation and activation energy on the axisymmetric rotating flow of Oldroyd-B fluid", *Phys. A Stat. Mech. its Appl.*, **580**, p. 124085 (2021). https://doi.org/10.1016/J.PHYSA.2019.124085
8. Shivakumara, I.S. and Sureshkumar, S., "Effects of throughflow and quadratic drag on the stability of a doubly diffusive Oldroyd-B fluid-saturated porous layer", *J. Geophys. Eng.*, **5**(3), pp. 268–280 (2008). https://doi.org/10.1088/1742-2132/5/3/003
9. Mahanthesh, B., Shashikumar, N.S., Gireesha, B.J., et al. "Effectiveness of Hall current and exponential heat source on unsteady heat transport of dusty TiO2-EO

nanoliquid with nonlinear radiative heat", *J. Comput. Des. Eng.*, **6**(4), pp. 551–561 (2019). https://doi.org/10.1016/J.JCDE.2019.04.005

10. Khan, M.I., Qayyum, S., Chu, Y.M., et al. "Transportation of Marangoni convection and irregular heat source in entropy optimized dissipative flow", *Int. Commun. Heat Mass Transf.*, **120**, p. 105031 (2021). https://doi.org/10.1016/J.ICHEATMASSTRANSFER.2020.105031
11. Mahanthesh, B., Gireesha, B.J., Animasaun, I.L., et al. "MHD flow of SWCNT and MWCNT nanoliquids past a rotating stretchable disk with thermal and exponential space dependent heat source", *Phys. Scr.*, **94**(8), p. 085214 (2019). https://doi.org/10.1088/1402-4896/AB18BA
12. Fatehinasab, R., Shafiee, H., Afshari, M., et al. "Hybrid surveying of radiation and magnetic impacts on Maxwell fluid with MWCNT nanotube influence of two wire loops", *ZAMM - J. Appl. Math. Mech. / Zeitschrift für Angew. Math. und Mech.*, **103**(1), e202200186 (2023). https://doi.org/10.1002/ZAMM.202200186
13. Ferdosi, S., Mohammadyahya, N., and Abasi, M. "Axial buckling of single-walled nanotubes simulated by an atomistic finite element model under different temperatures and boundary conditions", *Int J Sci Eng App*, **11**(11). pp. 151-163, (2022). https://doi.org/10.7753/IJSEA1111.1002
14. Jakeer, S. and Bala Anki Reddy, P. "Entropy generation on EMHD stagnation point flow of hybrid nanofluid over a stretching sheet: Homotopy perturbation solution", *Phys. Scr.*, **95**(12), p. 125203 (2020). https://doi.org/10.1088/1402-4896/abc03c
15. Khan, M.I., Qayyum, S., Hayat, T., et al. "Entropy generation minimization and statistical declaration with probable error for skin friction coefficient and Nusselt number", *Chinese J. Phys.*, **56**(4), pp. 1525–1546 (2018). https://doi.org/10.1016/j.cjph.2018.06.023
16. Rashidi, M.M., Abelman, S., and Mehr, N.F., "Entropy generation in steady MHD flow due to a rotating porous disk in a nanofluid", *Int. J. Heat Mass Transf.*, **62**(1), pp. 515–525 (2013). https://doi.org/10.1016/j.ijheatmasstransfer.2013.03.004
17. Reddy, P.B.A. and Das, R. "Estimation of MHD boundary layer slip flow over a permeable stretching cylinder in the presence of chemical reaction through numerical and artificial neural network modeling", *Eng. Sci. Technol. an Int. J.*, **19**(3), pp. 1108–1116 (2016). https://doi.org/10.1016/j.jestch.2015.12.013
18. Raghu, S. and Sriraam, N. "Optimal configuration of multilayer perceptron neural network classifier for recognition of intracranial epileptic seizures", *Expert Syst. Appl.*, **89**, pp. 205–221 (2017). https://doi.org/10.1016/J.ESWA.2017.07.029
19. Hasan, T.T., Jasim, M.H., and Hashim, I.A., "Heart disease diagnosis system based on multi-layer perceptron neural network and support vector machine", *Int. J. Curr. Eng. Technol.*, **77**(55), pp. 2277–4106 (2017).
20. Heidari, A.A., Faris, H., Aljarah, I., et al. "An efficient hybrid multilayer perceptron neural network with grasshopper optimization", *Soft Comput.*, **23**(17), pp. 7941–7958 (2019). https://doi.org/10.1007/S00500-018-3424-2
21. Waris, A., Din, M., Ali, A., et al. "Green fabrication of Co and Co_3O_4nanoparticles and their biomedical applications: A review", *Open Life Sci.*, **16**(1), pp. 14–30 (2021). https://doi.org/10.1515/BIOL-2021-0003
22. Khan, M., Ali, W., and Ahmed, J. "A hybrid approach to study the influence of Hall current in radiative nanofluid flow over a rotating disk", *Appl. Nanosci.*, **10**(12), pp. 5167–5177 (2020). https://doi.org/10.1007/s13204-020-01415-w
23. Hafeez, A., Khan, M., and Ahmed, J. "Flow of Oldroyd-B fluid over a rotating disk with Cattaneo–Christov theory for heat and mass fluxes", *Comput. Methods Programs Biomed.*, **191**, p. 105374 (2020). https://doi.org/10.1016/j.cmpb.2020.105374
24. Hafeez, A., Khan, M., Ahmed, A., et al. "Rotational flow of Oldroyd-B nanofluid subject to Cattaneo-Christov double diffusion theory", *Appl. Math. Mech. (English Ed.)* **41**(7), pp. 1083–1094 (2020). https://doi.org/10.1007/s10483-020-2629-9
25. Ahmad, F., Gul, T., Khan, I., et al. "MHD thin film flow of the Oldroyd-B fluid together with bioconvection and activation energy", *Case Stud. Therm. Eng.*, **27**(July), 101218 (2021). https://doi.org/10.1016/j.csite.2021.101218
26. Mumraiz, S., Ali, A., Awais, M., et al. "Entropy generation in electrical magnetohydrodynamic flow of Al_2O_3–Cu/H_2O hybrid nanofluid with non-uniform heat flux", *J. Therm. Anal. Calorim.*, **143**, pp. 2135-2148 (June) (2020). https://doi.org/10.1007/s10973-020-09603-0
27. Reddy, P.B.A. "Biomedical aspects of entropy generation on electromagnetohydrodynamic blood flow of hybrid nanofluid with nonlinear thermal radiation and non-uniform heat source/sink", *Eur. Phys. J. Plus*, **135**(10), pp. 1–30 (2020). https://doi.org/10.1140/epjp/s13360-020-00825-7
28. Uddin, I., Ullah, I., Raja, M.A.Z., et al. "Design of intelligent computing networks for numerical treatment of thin film flow of Maxwell nanofluid over a stretched and rotating surface", *Surfaces and Interfaces*, **24**(February), 101107 (2021). https://doi.org/10.1016/j.surfin.2021.101107
29. Mustafa, I., Javed, T., and Ghaffari, A. "Heat transfer in MHD stagnation point flow of a ferrofluid over a stretchable rotating disk", *J. Mol. Liq.*, **219**, pp. 526–532 (2016). https://doi.org/10.1016/J.MOLLIQ.2016.03.046
30. Ahmed, J., Khan, M., Ahmad, L., et al. "Thermally radiative flow of Maxwell nanofluid over a permeable

rotating disk", *Phys. Scr.*, **94**(12), p. 125016 (2019). https://doi.org/10.1088/1402-4896/AB3B9A

31. Rashidi, M.M., Ali, M., Freidoonimehr, N., et al. "Parametric analysis and optimization of entropy generation in unsteady MHD flow over a stretching rotating disk using artificial neural network and particle swarm optimization algorithm", *Energy*, **55**, pp. 497–510 (2013). https://doi.org/10.1016/j.energy.2013.01.036
32. Asadi, S., Shahrabi, J., Abbaszadeh, P., et al. "A new hybrid artificial neural networks for rainfall–runoff process modeling", *Neurocomputing*, **121**, pp. 470–480 (2013). https://doi.org/10.1016/J.NEUCOM.2013.05.023
33. Seo, Y., Kim, S., Kisi, O., et al. "Daily water level forecasting using wavelet decomposition and artificial intelligence techniques", *J. Hydrol.*, **520**, pp. 224–243 (2015). https://doi.org/10.1016/J.JHYDROL.2014.11.050
34. Aichouri, I., Hani, A., Bougherira, N., et al. "River flow model using artificial neural networks", *Energy Procedia*, **74**, pp. 1007–1014 (2015). https://doi.org/10.1016/J.EGYPRO.2015.07.832
35. Toha, S.F., Tokhi, M.O., and Md Salleh, S. "Parametric modelling of a twin rotor system", *Mob. Robot. Solut. Challenges - Proc. 12th Int. Conf. Climbing Walk. Robot. Support Technol. Mob. Mach. CLAWAR 2009*, pp. 285–292 (2010). https://doi.org/10.1142/9789814291279_0037
36. Kumar, S., Indian, A., and Khan, Z. "Neural network model for prediction of ground water level in metropolitan considering rainfall-runoff as a parameter", *Int. J. Soft Comput. Eng.*, (**3**), pp. 2231–2307 (2013).
37. Hagan, M.T. and Menhaj, M.B., "Training Feedforward Networks with the Marquardt Algorithm", *IEEE Trans. Neural Networks*, **5**(6), pp. 989–993 (1994). https://doi.org/10.1109/72.329697

Biographies

Abbai Reddy Divya completed her PhD program at Vellore Institute of Technology, Vellore, Tamilnadu, India. She completed her MSc in the year 2013 PVKN college, Chittoor, Andhra Pradesh, India. Her research interests are fluid dynamics, boundary-layer theory, ANN.

Polu Bala Anki Reddy was born and brought up in Andhra Pradesh, India. He obtained the MSc and PhD degrees in Mathematics from the Sri Venkateswara University, Tirupati, Andhra Pradesh. Presently, he is working as an Associate Professor at the Department of Mathematics, Vellore Institute of Technology, Vellore, Tamilnadu. Dr. Reddy's research interest covers the application of flow separation, particularly in bio- fluid dynamics and analysis of boundary layer flows of Newtonian/non-Newtonian fluids including entropy generation. His research interest also covers the hybrid nanofluid flow with entropy generation. He has published several papers in national and international journals and attended several workshops/seminars/faculty development programs. Moreover, Reddy has been selected as the top 2% of scientists in the world by Stanford University, USA, and Elsevier BV for the year 2022.